

Article

Distinct Roles of Additives in the Improved Sensitivity to CO of Ag- and Pd-Modified Nanosized LaFeO₃

Valentina Chumakova¹, Artem Marikutsa^{1,*} , Vadim Platonov¹, Nikolay Khmelevsky² 
and Marina Rumyantseva¹ 

¹ Chemistry Department, Lomonosov Moscow State University, 1-3 Vorobyevy Gory, 119234 Moscow, Russia

² Material Properties Research Laboratory (LISM), Moscow State Technological University Stankin, Vadkovsky Ln. 1, 127055 Moscow, Russia

* Correspondence: artem.marikutsa@gmail.com; Tel.: +7-495-939-5471

Abstract: Perovskite-type mixed-metal oxides are of particular interest as semiconductor gas sensors due to the variability in the material composition and the stability of sensing parameters. LaFeO₃ is a *p*-type semiconductor with relatively high conductivity and gas sensitivity. However, less is known about the sensitivity and sensing mechanisms of LaFeO₃ modified by catalytic noble metals. In this work, we used a microwave-assisted sol-gel method to synthesize perovskite LaFeO₃ nanoparticles with an average size of 20–30 nm and a specific surface area of 6–8 m²/g. LaFeO₃ was modified by 2–5 wt.% Ag and Pd nanoparticles via the impregnation route. Using X-ray photoelectron spectroscopy, the additives were observed in the partially oxidized states Ag₂O/Ag and PdO/Pd, respectively. Electric conduction and sensitivity to noxious gases were characterized by electrophysical measurements. It was shown that LaFeO₃ modified by Ag and Pd had improved sensitivity and selectivity to CO, and the sensing behavior persisted in a wide range of relative humidity. Pristine and Ag-modified LaFeO₃ had the maximum sensitivity to CO at a temperature of 200 °C, while modification with Pd resulted in a decreased optimal operating temperature of 150 °C. In situ infrared spectroscopy revealed that supported Pd nanoparticles specifically catalyzed CO oxidation at the surface of LaFeO₃ at room temperature, which was the likely reason for the improved sensitivity and decreased optimal operating temperature of LaFeO₃/Pd sensors. On the other hand, Ag nanoparticles were deduced to activate CO oxidation by lattice oxygen at the surface of LaFeO₃, providing enhanced CO sensitivity at a higher temperature.

Keywords: lanthanum ferrite; gas sensor; palladium; silver; catalytic nanoparticles; carbon oxide; sensing mechanism; diffuse-reflectance infrared spectroscopy



Citation: Chumakova, V.; Marikutsa, A.; Platonov, V.; Khmelevsky, N.; Rumyantseva, M. Distinct Roles of Additives in the Improved Sensitivity to CO of Ag- and Pd-Modified Nanosized LaFeO₃. *Chemosensors* **2023**, *11*, 60. <https://doi.org/10.3390/chemosensors11010060>

Academic Editor: Pi-Guey Su

Received: 20 December 2022

Revised: 3 January 2023

Accepted: 11 January 2023

Published: 13 January 2023



Copyright: © 2023 by the authors. Licensee MDPI, Basel, Switzerland. This article is an open access article distributed under the terms and conditions of the Creative Commons Attribution (CC BY) license (<https://creativecommons.org/licenses/by/4.0/>).

1. Introduction

Semiconductor gas sensors are of practical interest for air quality monitoring and detecting noxious gases such as CO, NH₃, H₂S, etc., at the ppm–ppb concentration level. The sensors' operation principle is based on a reversible electric resistance change as a result of the chemisorption of target molecules and/or redox reactions with the surface oxygen of semiconductor oxides [1–3]. Mixed-metal oxides with the composition ABO₃ (A—cations of alkali, alkaline-earth or rare-earth metals; B—cations of transition or post-transition metals) with the perovskite structure are distinguished as a specific family of semiconductor sensors, which have been extensively studied [4,5]. The perovskite structure consists of a three-dimensional framework of corner-shared BO₆ octahedrons and A cations filling the cuboctahedral voids. The variability in the chemical composition of perovskites is due to the possibility of the partial or total substitution of A and B cations, provided that the ratios of the cation radii fit the Goldschmidt tolerance factor [6]. The perovskite structure undergoes distortions when the tolerance factor is not unity, but its behavior is also persistent for partially nonstoichiometric ABO₃ compounds with respect to cations

or oxygen [6,7]. The variability in the chemical composition, crystal structural distortion and point defects in perovskites makes it possible to control the electrophysical properties, surface reactivity and sensing behavior of the materials [8]. This is an advantage of ABO_3 perovskites compared to simple semiconductor oxides.

Lanthanum ferrite ($LaFeO_3$) is a perovskite-structured *p*-type semiconductor with a bandgap width of 2.1 eV [9,10]. It has been extensively researched as a material for photocatalysts, catalysts and gas sensors [9–12]. $LaFeO_3$ has a relatively low resistance compared to other perovskite oxides ($107\text{--}108\text{ Ohm}\cdot\text{cm}^{-1}$ at room temperature), which is advantageous for semiconductor sensors [10,11]. $LaFeO_3$ was shown to be sensitive to oxidizing and reducing gases [12–18]. Spectroscopic studies of $LaFeO_3$ sensing mechanisms suggested that surface lattice oxygen anions and metal cations are the active sites responsible for the adsorption and redox conversion of target molecules [19]. La^{3+} cations stabilize Lewis base O^{2-} anions, which act as adsorption sites for acidic molecules. Fe^{3+} cations can partially change the oxidation state, controlling the adsorption–desorption equilibrium between lattice oxygen anions, oxygen vacancies and gas-phase oxygen. It accounts for redox interactions with oxidizing and reducing target gases [19,20]. The modification of semiconductor perovskite oxides with catalytic nanoparticles of noble metals, for example, Ag and Pd, is an efficient approach for improving the sensitivity and selectivity to reducing gases [17,18,21]. The role of noble metal additives in improving the sensing behavior has conventionally been explained by electronic interactions with the semiconductor oxide or by the catalytic effect on oxygen adsorption and spillover at the noble metal nanoparticles [22]. However, the sensing mechanisms of composites based on noble-metal-loaded $LaFeO_3$ have been less studied and understood.

The aim of the present work is to comparatively study the gas-sensing behavior and sensing mechanisms of nanocomposites based on $LaFeO_3$ with catalytic nanoparticles of Pd and Ag. Nanocrystalline $LaFeO_3$ was obtained via the microwave-assisted sol–gel method and modified by different concentrations of Ag and Pd via the impregnation route. Increased sensitivity and selectivity to CO at different operating temperatures were observed for the catalytically modified composites. In situ diffuse-reflectance infrared Fourier transform spectroscopy (DRIFT) was used to unveil the CO-sensing mechanism of Ag- and Pd-modified $LaFeO_3$ materials. It was deduced that Pd selectively catalyzed CO conversion at about room temperature, improving the low-temperature sensitivity. Ag nanoparticles were efficient in the activation of the lattice oxygen reaction with target gas molecules at the surface of $LaFeO_3$, thereby increasing the sensitivity of the composite to CO at a higher temperature.

2. Materials and Methods

2.1. Materials Synthesis

Nanocrystalline lanthanum ferrite $LaFeO_3$ was synthesized by the sol–gel method, as was reported in [17]. Pure analytical-grade lanthanum nitrate hexahydrate $La(NO_3)_3\cdot 6H_2O$ and iron(III) nitrate nonahydrate $Fe(NO_3)_3\cdot 9H_2O$ (Reachem, Moscow, Russia) were used as precursors, and ethylenediamine ($C_2H_8N_2$) was used as a complexing agent. Three solutions were prepared, 0.8 M $La(NO_3)_3\cdot 6H_2O$, 0.8 M $Fe(NO_3)_3\cdot 9H_2O$ and 2.5 M $C_2H_8N_2$, in absolute ethanol and stirred for 20 min. The solutions were mixed and the resultant mixture was stirred for 24 h at room temperature until pH = 7 was reached. The obtained sol was kept in a microwave oven (145 W) until a gel formed and the solvent partially evaporated. The residual gel was dried at 80 °C for 3 h until the solvent completely evaporated and at 200 °C for 8 h. The dried xerogel was annealed in air at 600 °C for 9 h.

Modification with silver (Ag) and palladium (Pd) (2–5 wt.%) was performed using the impregnation technique. First, 1 M aqueous solutions of silver nitrate $AgNO_3$ (Reachem, Moscow, Russia) and palladium(II) acetylacetonate $Pd(acac)_2$ (Sigma-Aldrich, St. Louis, MO, USA) were prepared and mixed with two parts of $LaFeO_3$ powder. The obtained suspensions were dried at 90 °C and annealed in air for 3 h to decompose the noble metal precursors at 300 °C ($LaFeO_3/Pd(acac)_2$) and at 400 °C ($LaFeO_3/AgNO_3$).

2.2. Materials Characterization

X-ray diffraction was measured on a DRON-3M diffractometer (CoK α radiation; $\lambda = 1.7903 \text{ \AA}$; angles $2\theta = 20\text{--}80^\circ$). Crystallite size was estimated by the Scherrer equation from the full-width-half-maxima of the 3 most intense peaks. The specific surface area was determined by the BET method using the Chemisorb 2750 setup (Micrometrics, Norcross, GA, USA). Before measurements, samples were pretreated at 300°C for 30 min in He ambient and then cooled to room temperature. The morphology of the powders was studied by scanning electron microscopy (SEM) using a Carl Zeiss SUPRA 40 FE-SEM microscope (Carl Zeiss AG, Oberkochen, Germany) with an Inlens SE detector at an accelerating voltage of 5 kV and an aperture of 30 microns.

The elemental composition was determined by X-ray fluorescence (XRF) using the M1 MISTRAL device (Bruker, Billerica, MA, United States) (voltage 50 kV; current 800 μA). X-ray photoelectron spectra (XPS) were registered using the Axis Ultra DLD instrument (Kratos, Manchester, UK). The measurements were carried out with an Al K α source, and the binding energy was calibrated to the C 1s signal (285.0 eV).

Fourier transform infrared spectra in transmission (FTIR) and diffuse-reflectance mode (DRIFT) were registered using a Frontier spectrometer with automatic CO₂/H₂O compensation and a resolution of 4 cm^{-1} (Perkin Elmer, Waltham, MA, USA). FTIR spectra were acquired using pellets of samples diluted with KBr in the wavenumber range of $4000\text{--}400 \text{ cm}^{-1}$ with the accumulation of 4 scans. DRIFT spectra were collected using the DiffuseIR annex equipped with an HC900 chamber sealed by a KBr window (Pike, Fitchburg, WI, USA). Powders were put into a sapphire crucible (6 mm diameter, 4 mm height) and pretreated at 200°C under a flow of dry air to desorb humidity. DRIFT spectra were measured with the accumulation of 30 scans during the in situ exposure of samples to the target gas (400 ppm CO) at room temperature and at 200°C . Background spectra were preliminarily registered under a flow of dry air at the corresponding temperature.

To prepare the sensors, the samples (~5 mg) were ground in terpineol (20 mL), and the obtained paste was deposited onto alumina substrates (size $0.3 \times 0.2 \text{ mm}^2$) with interdigitated platinum heaters and contacts. Microhotplates were assembled at the Moscow Engineering Physics Institute. The formed thick films (5–10 microns) were annealed at 300°C for 10 h in air to remove the organic binder. Sensing tests were performed by taking in situ electrophysical measurements in a gas flow chamber assembled with an electrometer. Sensor responses were measured at temperatures of $50\text{--}500^\circ\text{C}$ for pristine LaFeO₃, $50\text{--}400^\circ\text{C}$ for LaFeO₃/Ag and $50\text{--}300^\circ\text{C}$ for LaFeO₃/Pd, i.e., not exceeding the annealing temperature of the composites so as to prevent the undesired morphology failure of noble metal nanoparticles. Certified gas mixtures of CO:N₂ ($5120 \pm 50 \text{ ppm}$), NH₃:N₂ ($1100 \pm 10 \text{ ppm}$), NO₂:N₂ ($96 \pm 6 \text{ ppm}$) and H₂S:N₂ ($51 \pm 5 \text{ ppm}$) were used as the sources of target gases. Purified dry air from the generator of pure air (GPA-1.2-3.5, Khimelectronica, Moscow, Russia) was used as a carrier and reference gas. Gas flows were controlled by EL-FLOW mass-flow controllers (Bronkhorst, Ruurlo, The Netherlands). The overall gas flow rate was kept constant (100 mL/min), and the target gases were diluted with pure air to prepare target gas mixtures with certain concentrations.

3. Results

3.1. Composition and Structure of Materials

According to X-ray diffraction (Figure 1), the obtained LaFeO₃ consisted of a single phase with a perovskite-like orthorhombic Pbnm structure (ICDD# 74-2203). No palladium-related crystalline phases were observed in the LaFeO₃/Pd composites. This may be due to the amorphous state or small nanoparticle size of the additive. In the Ag-modified composites, the phase of metallic Ag with a cubic structure (ICDD# 4-783) was observed along with the orthorhombic perovskite phase of LaFeO₃ (Figure 1). The crystallites sizes estimated by the Scherrer equation were in the ranges of $d_{\text{XRD}} = 19\text{--}28 \text{ nm}$ for LaFeO₃ in all the samples and about $d_{\text{XRD}} = 27\text{--}43 \text{ nm}$ for the Ag phase in the LaFeO₃/Ag composites (Table 1). In the XRD patterns of LaFeO₃/Ag and LaFeO₃/Pd composites, no peak shifts

of the perovskite phase were observed relative to pristine LaFeO₃. This indicates that the cations of the additives (silver or palladium) were not incorporated into the crystal lattice of the host perovskite LaFeO₃. The BET surface area was similar for all samples and in the range of 6–8 m²/g.

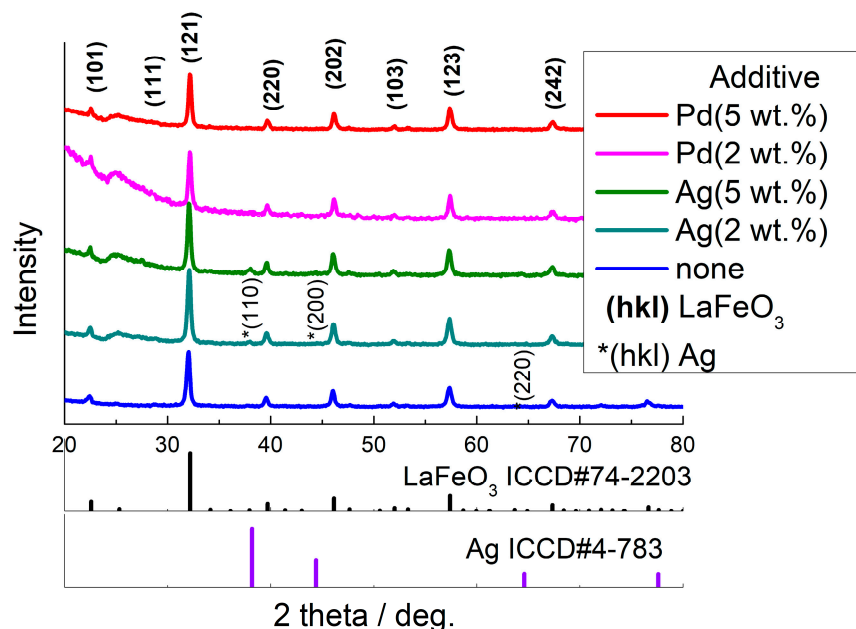


Figure 1. XRD patterns of pristine and Ag- or Pd-modified LaFeO₃.

Table 1. Composition and microstructural parameters of materials.

Sample	Percentage of Additive, wt.%	Crystallite Size (d_{XRD}), nm	BET Area, m ² /g
LaFeO ₃	-	23 ± 4	8
LaFeO ₃ /Ag(2 wt.%)	2.1 ± 0.2 Ag	24 ± 4 LaFeO ₃ ; 37 ± 6 Ag	6
LaFeO ₃ /Ag(5 wt.%)	4.9 ± 0.3 Ag	23 ± 4 LaFeO ₃ ; 32 ± 5 Ag	6
LaFeO ₃ /Pd(2 wt.%)	2.2 ± 0.2 Pd	24 ± 5 LaFeO ₃	7
LaFeO ₃ /Pd(5 wt.%)	5.1 ± 0.4 Pd	23 ± 4 LaFeO ₃	6

In the SEM images (Figure 2), nanoparticles with average sizes in the range of 20–50 nm were distinguished, which is in agreement with the crystallite sizes of LaFeO₃ and Ag estimated by XRD. The morphologies of pristine and modified LaFeO₃ samples were represented by isotropically shaped irregular nanoparticles. The nanoparticles were strongly agglomerated into loose three-dimensional aggregates (Figure 2a). The modifiers, which were presumably segregated at the surface of LaFeO₃, could not be distinguished in the SEM images (Figure 2b–d), likely because of the close nanoparticle sizes of the perovskite support and of the additives. This agrees with the XRD data on the crystallite size of LaFeO₃ and Ag (Table 1). Moreover, the close atomic numbers of Ag and Pd are intermediate between those of La and Fe, and the additives could not be distinguished by contrast from the background of LaFeO₃.

Quantitative elemental analysis by XRF showed that the La/Fe ratio was 1.07 ± 0.13 in the samples, which corresponds to the stoichiometric composition of perovskite LaFeO₃ (Supplementary Data). The estimated concentrations of Ag and Pd agree with the amounts used during the syntheses (Table 1).

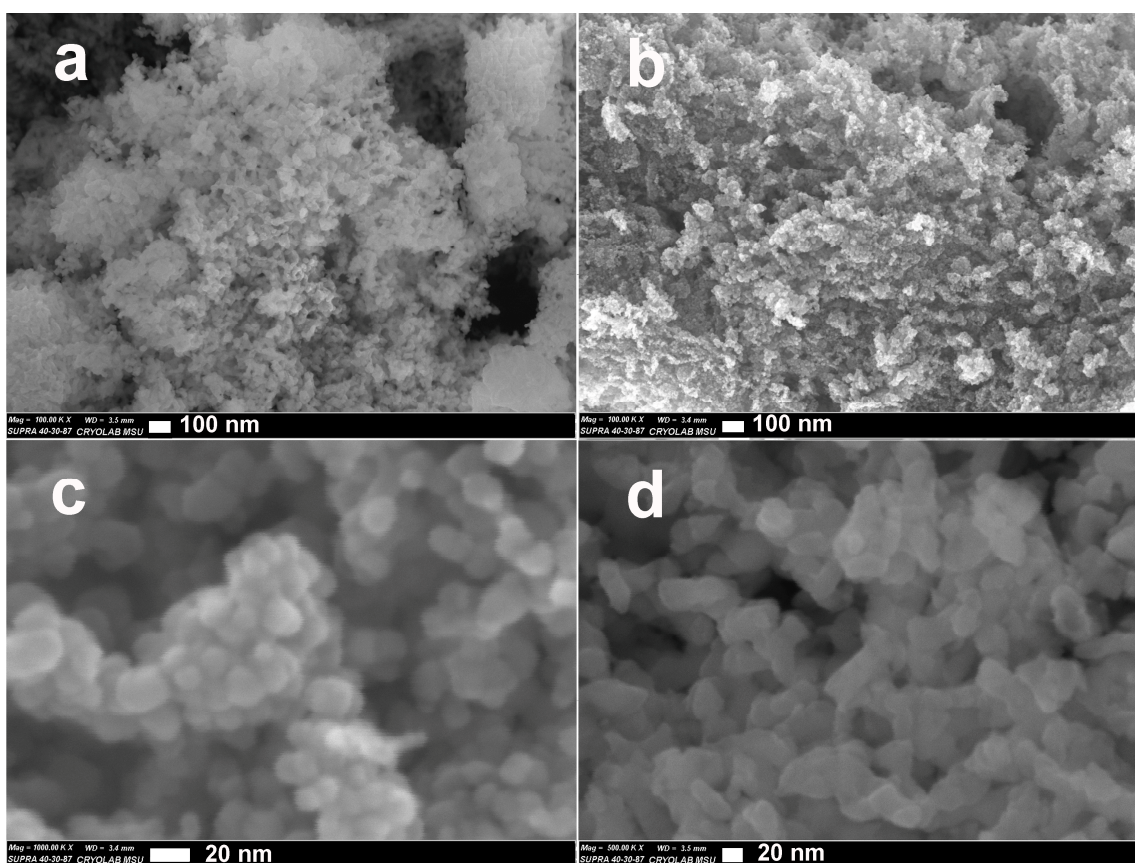


Figure 2. SEM images of LaFeO₃ (a), LaFeO₃/Ag(5 wt.%) (b), LaFeO₃/Pd(2 wt.%) (c) and LaFeO₃/Pd(5 wt.%) (d).

3.2. Oxidation States of Elements and Surface Species in the Materials

X-ray photoelectron (XP) spectra displayed the spin-orbit split doublet signals of La 3d and Fe 2p, with binding energies (BE) corresponding to the oxidation states La³⁺ and Fe³⁺ in pristine and modified LaFeO₃ samples (Figure 3a,b) [23,24]. No effects of Ag or Pd on the oxidation states of cations in the perovskite structure were observed. XP spectra of the Ag 3d level showed that silver was in two oxidation states in the LaFeO₃/Ag composites (Figure 3c). One was Ag⁰ with BE(Ag 3d_{5/2}) = 368.7–369.0 eV, which is consistent with the presence of metallic silver nanoparticles in the composites observed by XRD. The other state was Ag⁺ with BE(Ag 3d_{5/2}) = 367.8–368.1 eV [25]. Likely, the oxidized Ag₂O layer was formed at the surface of Ag nanoparticles as a result of the interaction with gas-phase oxygen. Similarly, palladium was found in two oxidation states in the LaFeO₃/Pd composites: Pd⁰ with BE(Pd 3d_{5/2}) = 335.0–335.3 eV and Pd²⁺ with BE(Pd 3d_{5/2}) = 336.6–336.9 eV (Figure 3d). The relative atomic concentrations of the reduced and oxidized forms of noble metal additives estimated from the curve-fitted XP spectra are summarized in Table 2. In the Ag-modified samples, metallic silver was the predominant form (68–76 at.% of total Ag content). On the contrary, in the LaFeO₃/Pd composites, the concentration of the oxidized form Pd²⁺ (63–66 at.% of total Pd content) exceeded that of the reduced form Pd⁰. With the increasing percentage of additives in LaFeO₃, the fraction of M⁰ (M = Ag, Pd) increases.

The XP spectra of the O 1s level were contributed to by three components corresponding to oxygen anions in the structure of LaFeO₃, labeled as O(I) with BE = 529.2–529.7 eV, and oxygen in adsorbed surface species (Figure 3e). According to FTIR data, the latter may be recognized as carbonate groups with the O(II) state (BE = 531.2–531.8 eV) and hydroxyl groups possessing the O(III) state (BE = 533.4–534.1 eV) [26]. The highest intensity was observed for the O(II) component, i.e., oxygen of the surface carbonate groups, which might originate from CO₂ adsorption to the surface of LaFeO₃. In the Ag-modified samples, the

atomic ratio of different components in the O 1s spectrum did not change in comparison to pristine LaFeO₃ (Table 2). However, when the Pd additive was introduced, the fraction of surface carbonate groups decreased, and the fraction of OH groups increased.

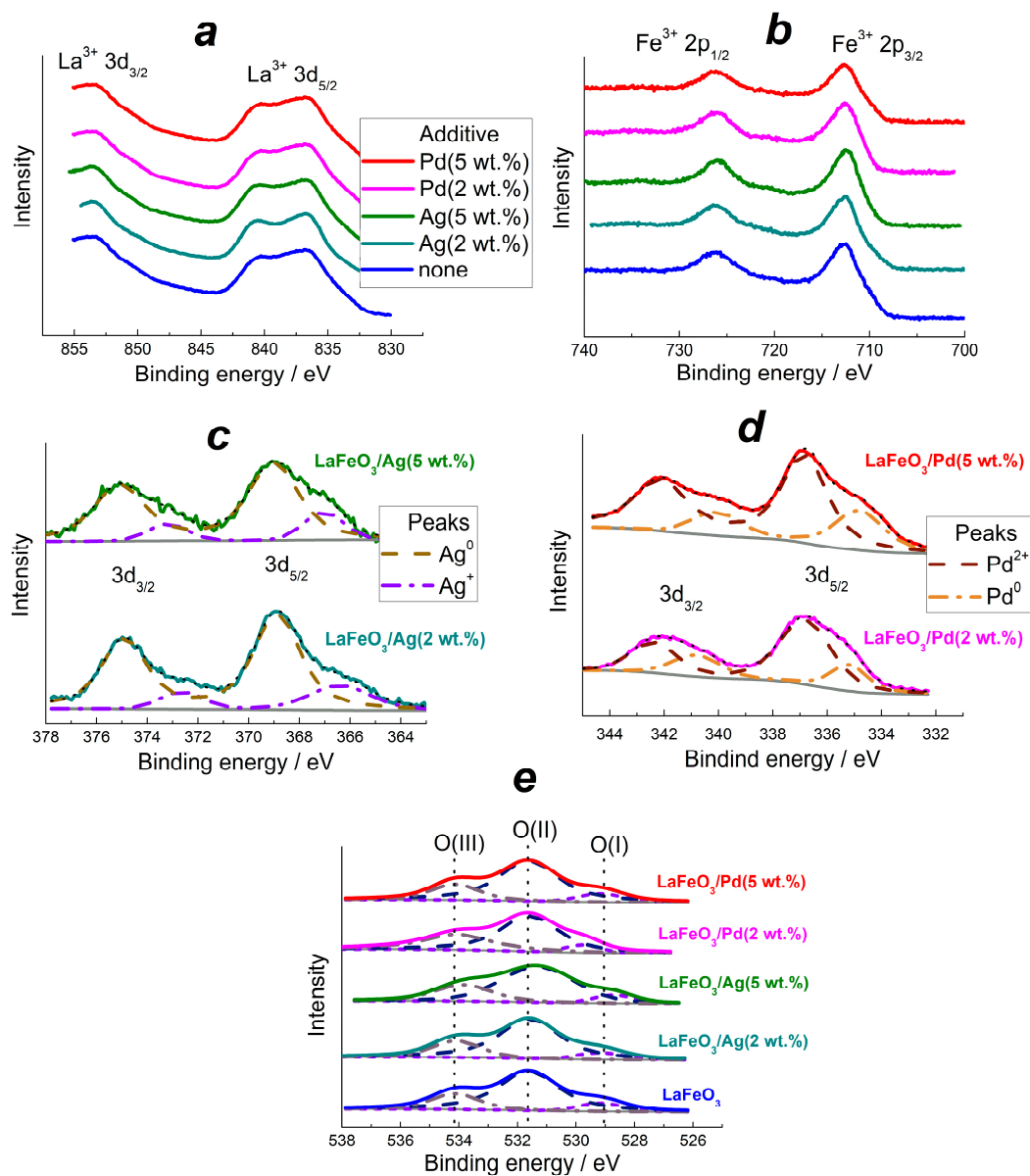


Figure 3. XPS spectra of pristine and Ag- or Pd-modified LaFeO₃ in the analytical regions of La 3d (a), Fe 2p (b), Ag 3d (c), Pd 3d (d) and O 1s (e).

Table 2. Relative fractions of oxidized (Mⁿ⁺) and reduced (M⁰) states of noble metals in Ag- and Pd-modified LaFeO₃ and of different states of oxygen in the materials determined by XPS.

Sample	Fraction from Total Content of the Element, at.%				
	M ⁿ⁺	M ⁰	O(I)	O(II)	O(III)
LaFeO ₃	-	-	18	52	30
LaFeO ₃ /Ag(2 wt.%)	24 (Ag ⁺)	76 (Ag ⁰)	17	57	26
LaFeO ₃ /Ag(5 wt.%)	32 (Ag ⁺)	68 (Ag ⁰)	12	60	29
LaFeO ₃ /Pd(2 wt.%)	63 (Pd ²⁺)	37 (Pd ⁰)	15	43	42
LaFeO ₃ /Pd(5 wt.%)	66 (Pd ²⁺)	34 (Pd ⁰)	16	38	46

The FTIR spectra of samples are dominated by the Fe-O stretching vibration band at 565 cm^{-1} related to the perovskite phase of LaFeO_3 (Figure 4) [27]. Minor bands of O-H stretching (3430 cm^{-1}) and H_2O bending vibrations (1630 cm^{-1}) were observed due to adsorbed water. The peaks at 1490 cm^{-1} , 1370 cm^{-1} and 860 cm^{-1} can be ascribed to monodentate carbonate species because of CO_2 adsorption [28]. The relative intensities of carbonate peaks were a little stronger in the Ag-modified samples in comparison to LaFeO_3 and LaFeO_3/Pd (Supplementary Data, Figure S2).

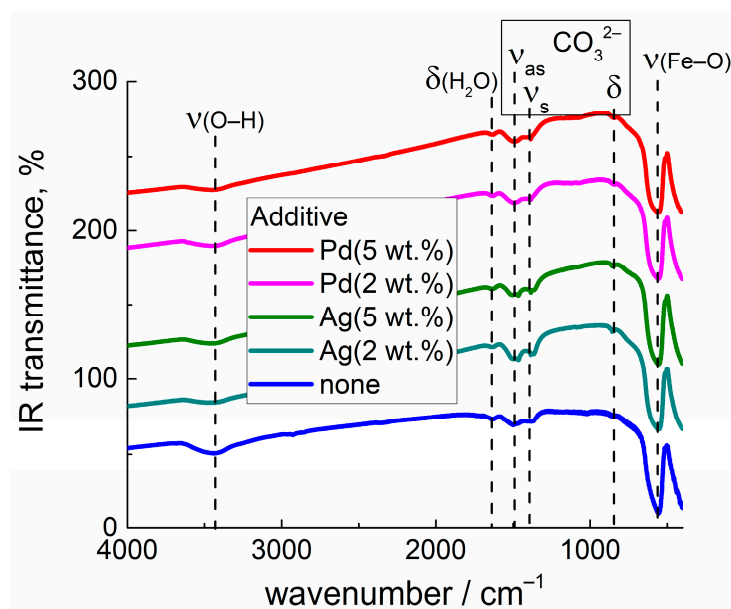


Figure 4. FTIR spectra of pristine and Ag- or Pd-modified LaFeO_3 .

3.3. Electrophysical and Gas-Sensing Properties

Figure 5 shows temperature plots of the DC resistance of pristine and modified LaFeO_3 . The materials behaved as semiconductors, and the resistance steadily dropped with rising temperature. Linear relations were observed in the coordinates $\lg R \sim 1/T$, indicating the activation character of conductance. The estimated effective activation energies of conduction are summarized in Table 3. At a temperature of around $450\text{ }^\circ\text{C}$, an inclination was observed on the linear plot of LaFeO_3 , which can be associated with a change in magnetic ordering. This can be a transition from the antiferromagnetic to the paramagnetic state of LaFeO_3 , since the Neel temperature $T_N = 462\text{ }^\circ\text{C}$ was reported for lanthanum ferrite [29,30]. This transition at temperature $T > T_N$ is accompanied by a decrease in the activation energy of conduction (Table 3).

When LaFeO_3 was modified by Ag or Pd, the resistance increased with the concentration of the additive. This should be due to the formation of the hole-depleted Schottky barrier at the semiconductor/noble metal interface. The work functions of Ag, Ag_2O , Pd, PdO and LaFeO_3 are 4.7, 5.0, 4.8, 6.0 and 6.5 eV, respectively [31–34]. When the heterojunction is formed between the *p*-type LaFeO_3 semiconductor and nanoparticles of $\text{Ag}_2\text{O}/\text{Ag}$ or PdO/Pd, an electronic transfer would be expected from introducing the additives to LaFeO_3 . This leads to a decrease in the concentration of holes, which are the charge carriers in lanthanum ferrite, and the formation of a potential barrier for hole conduction. For the sake of simplicity, we assumed metallic behavior for the partially oxidized noble metal additives, and the position of the Fermi energy level is described by the work function between the work function limits of completely oxidized and completely reduced noble metals. According to the Schottky–Mott model of the metal–semiconductor heterojunction, the potential energy barrier for hole conduction arises at the interface, and its height is characterized by the difference $E_F - E_v$. Here, E_F is the energy of the Fermi level, which

is aligned between the contacting metal and semiconductor, and E_v is the energy of the valence band edge at the surface of LaFeO_3 , which is 6.8 eV below the vacuum level [9].

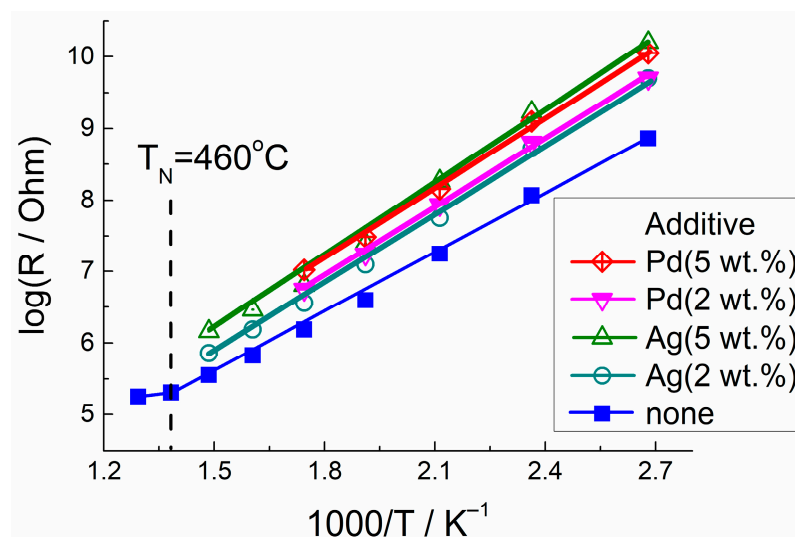


Figure 5. Logarithm of resistance of pristine and Ag- or Pd-modified LaFeO_3 in air in relation to inverse temperature.

Table 3. Effective activation energy of conduction of LaFeO_3 at lower ($T = 50\text{--}450\text{ }^\circ\text{C}$) and higher ($T = 450\text{--}500\text{ }^\circ\text{C}$) temperature ranges and of Ag- and Pd-modified LaFeO_3 at tested temperatures ($T = 50\text{--}400\text{ }^\circ\text{C}$ and $T = 50\text{--}300\text{ }^\circ\text{C}$, respectively).

Sample	Activation Energy of Conduction, eV	
	Lower Temperature	Higher Temperature
LaFeO_3	0.55 ± 0.02	0.13 ± 0.02
$\text{LaFeO}_3/\text{Ag}(2\text{ wt.}\%)$	0.61 ± 0.02	
$\text{LaFeO}_3/\text{Ag}(5\text{ wt.}\%)$	0.66 ± 0.03	
$\text{LaFeO}_3/\text{Pd}(2\text{ wt.}\%)$	0.61 ± 0.02	
$\text{LaFeO}_3/\text{Pd}(5\text{ wt.}\%)$	0.63 ± 0.02	

The sensing behavior was investigated using different reducing gases (CO , NH_3 , H_2S and CH_3COCH_3) and an oxidizing gas (NO_2). Figure 6a shows the dynamic response of LaFeO_3 to CO (20 ppm) and NO_2 (1 ppm). All sensors demonstrated *p*-type responses: i.e., resistance reversibly increased in the presence of reducing gases and decreased in the presence of the oxidizing gas. Sensor signals were calculated by determining the relative change in sensor resistance:

$$S = 100\% \cdot (R_{\text{gas}} - R_{\text{air}}) / R_{\text{air}} \text{ (to reducing gases);}$$

$$S = 100\% \cdot (R_{\text{air}} - R_{\text{NO}_2}) / R_{\text{NO}_2} \text{ (to oxidizing gas)} \quad (1)$$

where R_{air} is sensors resistance in air, and R_{gas} is resistance in the presence of the target gas. The temperature dependences of sensor signals are shown in Figure 7. For pristine LaFeO_3 , the optimal operating temperature for detecting CO was $T = 200\text{ }^\circ\text{C}$, for sensing H_2S and NO_2 , it was $T = 250\text{ }^\circ\text{C}$, and for detecting NH_3 , it was $T = 300\text{ }^\circ\text{C}$.

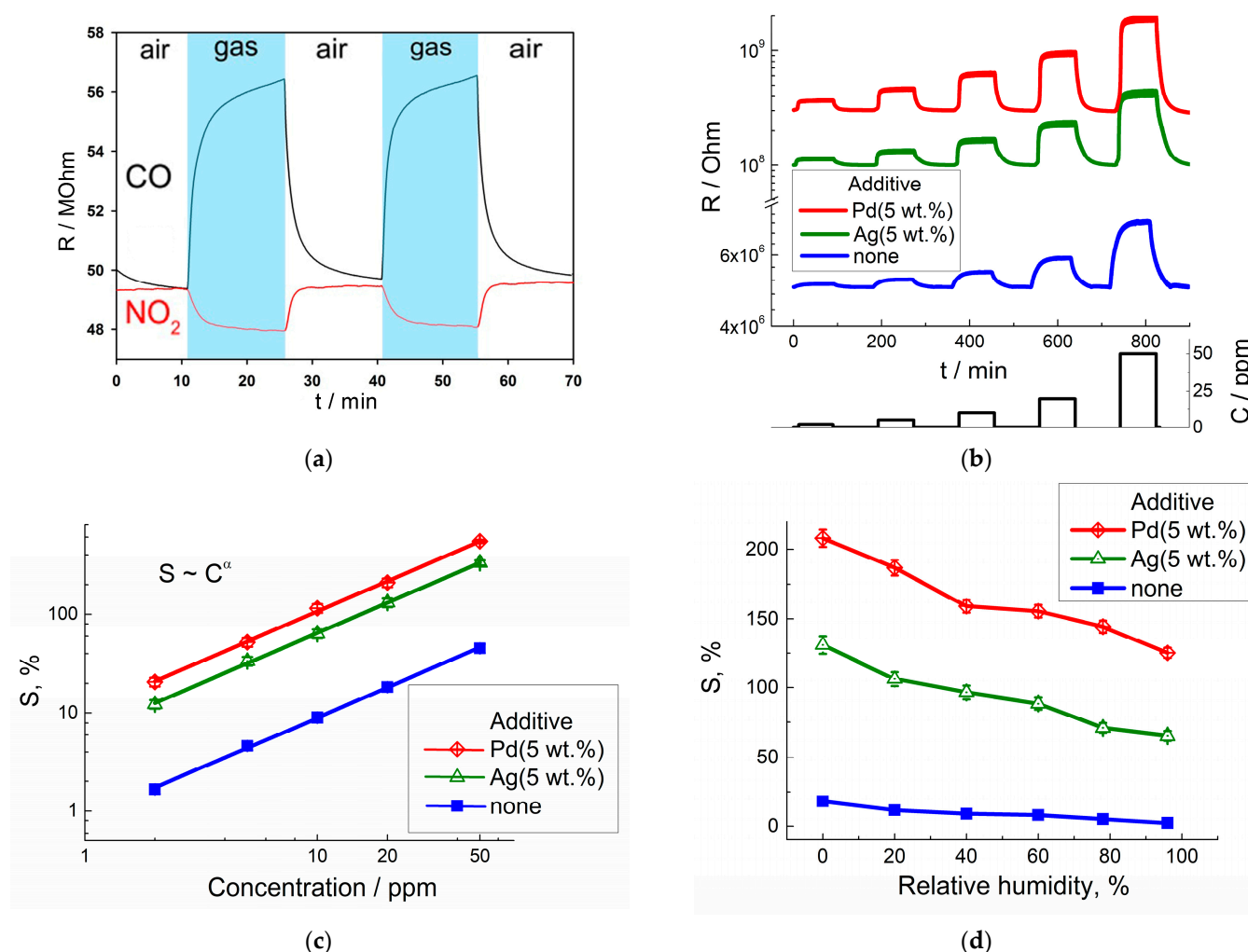


Figure 6. Dynamic sensor response of LaFeO₃ to 20 ppm CO and 1 ppm NO₂ at 200 °C (a); dynamic response to increasing concentration of CO for LaFeO₃ and LaFeO₃/Ag(5 wt.%) at 200 °C and for LaFeO₃/Pd(5 wt.%) at 150 °C (b); dependence of sensor signals on CO concentration for LaFeO₃ and LaFeO₃/Ag(5 wt.%) at 200 °C and for LaFeO₃/Pd(5 wt.%) at 150 °C (c); sensor signals of LaFeO₃ and LaFeO₃/Ag(5 wt.%) at 200 °C and for LaFeO₃/Pd(5 wt.%) at 150 °C to 20 ppm CO at different relative humidity levels (d).

Modification with Ag did not affect the temperature dependences of sensor signals, and the values of sensor signals only changed compared to LaFeO₃ (Figure 7). For the Pd-modified sensors, the optimal operating temperatures for sensing all target gases were 50 °C lower relative to pristine LaFeO₃. In all cases, the temperature corresponding to the maximum sensor signals of modified sensors was lower than the annealing temperature of LaFeO₃/Ag and LaFeO₃/Pd. This means that nanocomposites do not have to be continuously heated at high temperatures, which ensures stable and long-term sensor operation under optimal measurement conditions.

The selectivity of Ag- and Pd-modified LaFeO₃ sensors can be estimated from Figure 8. When LaFeO₃ was modified by Ag, an increased sensitivity to CO was observed, while the sensitivity to other gases did not exceed that of pristine LaFeO₃ (Figure 8a). The improved sensitivity of LaFeO₃/Ag to CO can be contributed to by the effect of electronic sensitization [2,3]. As shown by XPS, silver nanoparticles are partially oxidized to Ag₂O in the composites (Figure 3c). The interaction with CO should increase the fraction of reduced Ag in the initially partially oxidized Ag₂O/Ag additive. After the partial reduction by target gas molecules, the work function of reduced nanoparticles decreases, Fermi energy

increases and, hence, the height of the energy barrier for hole conduction increases. This is schematically represented in Figure 9. As a result, the concentration of charge carriers decreases in *p*-type semiconductors, and the resistance increases to a larger extent relative to pristine LaFeO₃. As the percentage of Ag increased from 2 wt.% to 5 wt.%, a further 2–3 increment in the sensitivity to CO was observed. This might be associated with the higher Ag⁺/Ag⁰ ratio in the Ag (5 wt.%) -modified sample (Table 2), implying more active Ag⁺ sites for the interaction with CO. However, the difference in the Ag⁺/Ag⁰ ratio between LaFeO₃/Ag (2 wt.%) and LaFeO₃/Ag (5 wt.%) was low, and comparable to the uncertainty in the curve fitting of XP spectra. Thus, the route of LaFeO₃ sensitization by the Ag additive cannot be ascribed only to the electronic effect, and more insights were obtained by DRIFT spectroscopy.

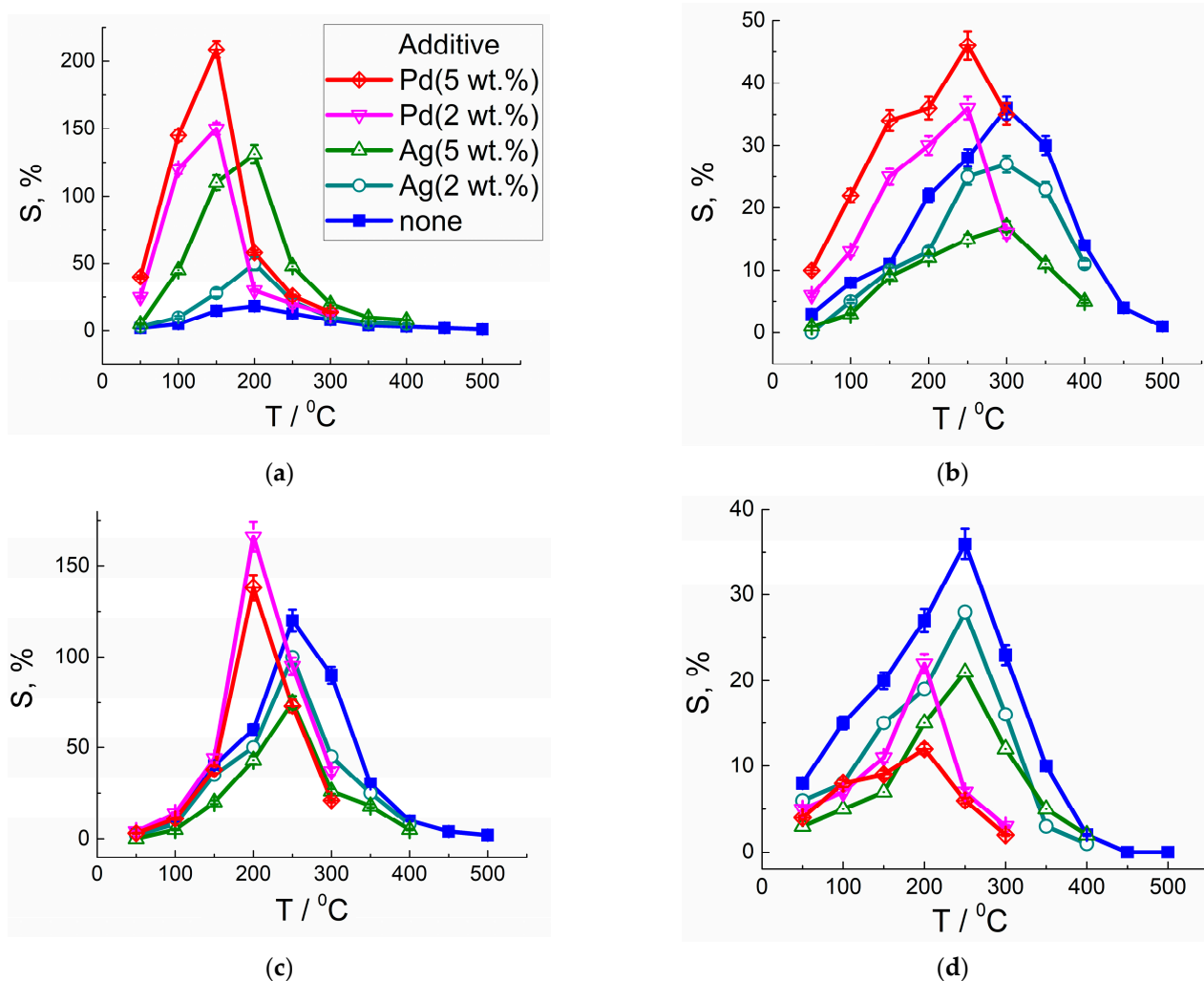


Figure 7. Temperature plots of sensor signals of pristine and Ag- or Pd-modified LaFeO₃ to 20 ppm CO (a), 20 ppm NH₃ (b), 2 ppm H₂S (c) and 1 ppm NO₂ (d).

The modification of LaFeO₃ with Pd slightly improved the sensitivity to all tested reducing gases, but an exceptionally large increase in sensor signals in response to CO was observed (Figure 8b). With the increase in Pd percentage from 2 wt.% to 5 wt.%, the sensitivity to CO increased, but to a lesser extent than in the case of LaFeO₃/Ag. The improved sensitivity to CO can be contributed to by the electronic effects at the additive/support interface (Figure 9). However, electronic sensitization does not explain the observed selectivity to CO and the lower optimal operating temperature of LaFeO₃/Pd.

The catalytic role of Pd in the conversion of CO (chemical sensitization) was deduced from a DRIFT spectroscopy study.

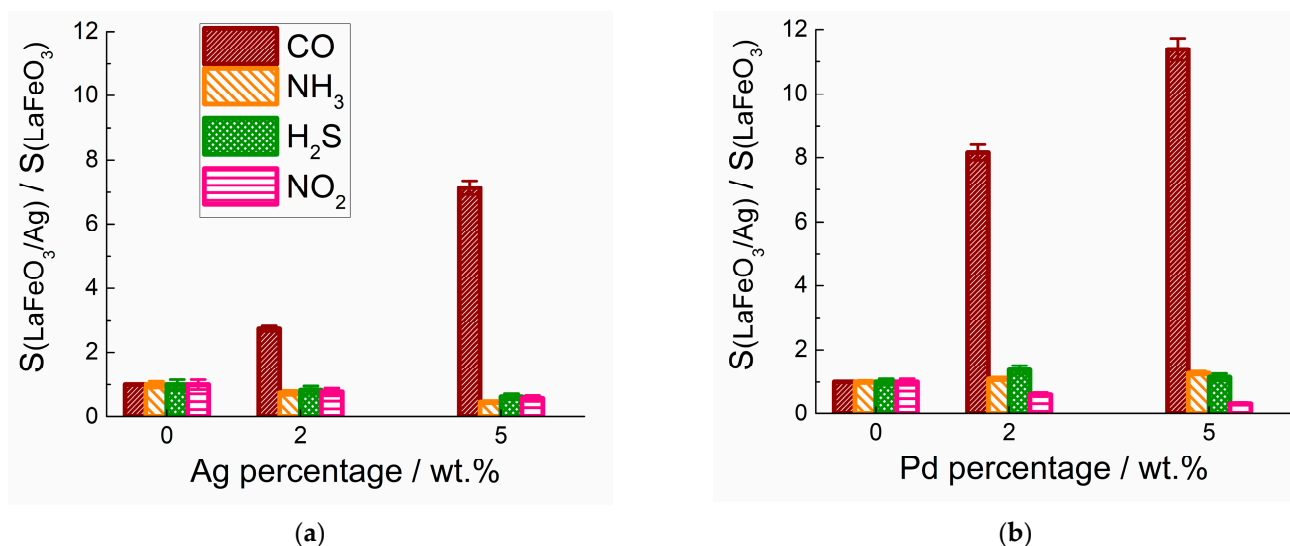


Figure 8. Ratio of maximum sensor signals of LaFeO₃/Ag (a) and LaFeO₃/Pd (b) to sensor signals of pristine LaFeO₃ to CO (20 ppm), NH₃ (20 ppm), H₂S (2 ppm) and NO₂ (1 ppm) at appropriate operating temperatures.

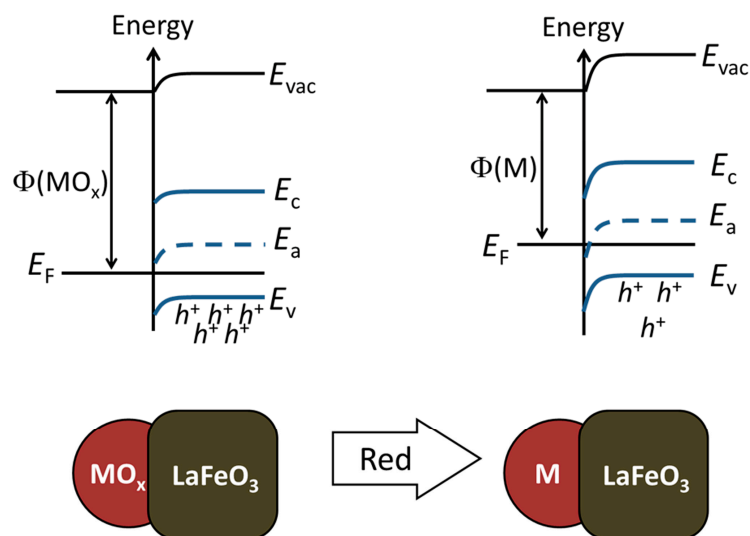


Figure 9. Scheme of electronic sensitization effect of LaFeO₃ by partially oxidized noble metals, where MO_x is Ag₂O/Ag or PdO/Pd, M is one of the reduced noble metals, E_{vac} is vacuum level, E_c is conduction band edge, E_a is acceptor level, E_v is valence band edge, and Φ is work function of oxidized and reduced noble metals.

The dependences of sensor signals on CO concentration are shown in Figure 6b. The sensors based on Ag- and Pd-modified LaFeO₃ are sensitive to as low as 2 ppm CO in air, which is below the threshold limit value (25 ppm 8-h TWA) [35]. The concentration dependences of sensor signals were linear in logarithmic coordinates, indicating the power law $S \sim C^\alpha$ (Figure 6c). The slope was close to unity at $\alpha = 1.01 \pm 0.01$ for all tested materials. The response (t_{res}) and recovery (t_{rec}) times, determined as the periods required for sensors to reach 90% of stable resistance in the target gas and in pure air, were $t_{\text{res}} = 1\text{--}2$ min and $t_{\text{rec}} = 5\text{--}7$ min for LaFeO₃ and LaFeO₃/Ag and $t_{\text{res}} = 3$ min and $t_{\text{rec}} = 10$ min for LaFeO₃/Pd in response to 20 ppm CO in dry air at optimal operating temperatures.

The effect of humidity on the sensitivity to CO was studied in the range of relative humidity RH = 0–95% (Figure 6d). In the presence of 95% RH, the sensor signals decreased by 1.3–1.5 times relative to dry air. The larger drop in the sensitivity of LaFeO₃/Pd could be due to the lower operating temperature (150 °C). However, the Ag- and Pd-modified samples still possessed reliable sensor responses to CO in humid air. The drop in sensitivity to reducing gases in the presence of humidity is a common issue of metal oxide sensors. The competitive adsorption of water in the molecular (H₂O) and/or dissociated forms (OH groups) blocks, to some extent, the active surface sites and prevents the redox interaction with CO target molecules.

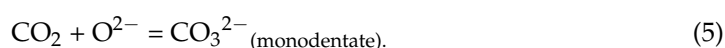
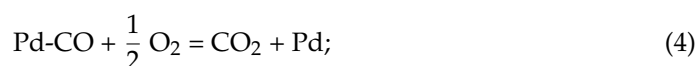
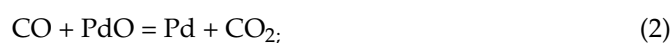
In Table 4, the characteristics of perovskite-based sensors in response to CO are summarized. The sensors based on LaFeO₃/Ag and LaFeO₃/Pd in the present work exhibit high sensitivity to relatively low CO concentrations and at lower operating temperatures in comparison to literature data.

Table 4. Comparison of resistive sensor parameters for perovskite-type mixed-metal oxides in the detection of CO gas.

Material	Synthesis Method	Morphology	CO Concentration, ppm	Operating T, °C	Sensor Signal, %	Ref.
LaFeO ₃	Sol-gel	Nanowires	50	250–270	25	[36]
rGO/LaFeO ₃	Hydrothermal	Microspheres	5	250	17	[27]
La _{1-x} Mg _x FeO ₃	Sol-gel	Nanofibers	2500	350	4000	[16]
La _{1-x} Sr _x FeO ₃	Sol-gel	Microspheres	50	400	2.5	[37]
LaFeO ₃	Coprecipitation	3D porous	1000	155	10	[14]
LaCoO ₃	PAD deposition	Thin films	100	150	55–80	[38]
LaCoO ₃ /Pd	Electrospinning	Nanowires	100	250	113	[21]
LaFeO ₃ /Ag	Sol-gel	Nanoparticles	20	200	130	This work
LaFeO ₃ /Pd	Sol-gel	Nanoparticles	20	150	210	

3.4. DRIFT Spectroscopy Study of Material Interaction with CO

The sensing mechanism was studied by DRIFT spectroscopy under in situ conditions simulating those of the sensing tests. Figure 10 shows the infrared absorbance spectra of materials exposed to 400 ppm CO referenced to pure air. At room temperature, minor spectral changes were observed for LaFeO₃ and LaFeO₃/Ag (Figure 10a). The positive band at 3400 cm⁻¹ and peak at 1640 cm⁻¹ correspond to the adsorption of H₂O and/or OH groups. This may be due to the presence of humidity in the source of the CO target gas and the low measurement temperature being favorable for water adsorption to the oxide surface. As observed in the spectra of Pd-modified LaFeO₃, exposure to CO resulted in decreased background absorbance and the appearance of a positive band at 3400 cm⁻¹ (O-H stretching vibrations) due to adsorbed humidity, a peak at 2335 cm⁻¹ and a strong doublet band at 1500–1400 cm⁻¹. The decline in the IR background can be due to a decreasing charge carrier concentration (holes), which agrees with the increasing resistance in the presence of CO (Figure 6a). The peak at 2335 cm⁻¹ should be due to asymmetric stretching vibrations of gas-phase CO₂, while the doublet at 1500–1400 cm⁻¹ can be ascribed to asymmetric and symmetric stretching vibrations of monodentate carbonate species. Thus, at room temperature, CO undergoes Pd-catalyzed conversion to CO₂, and the latter is adsorbed to the surface of perovskite in the form of monodentate CO₃²⁻ [28]:



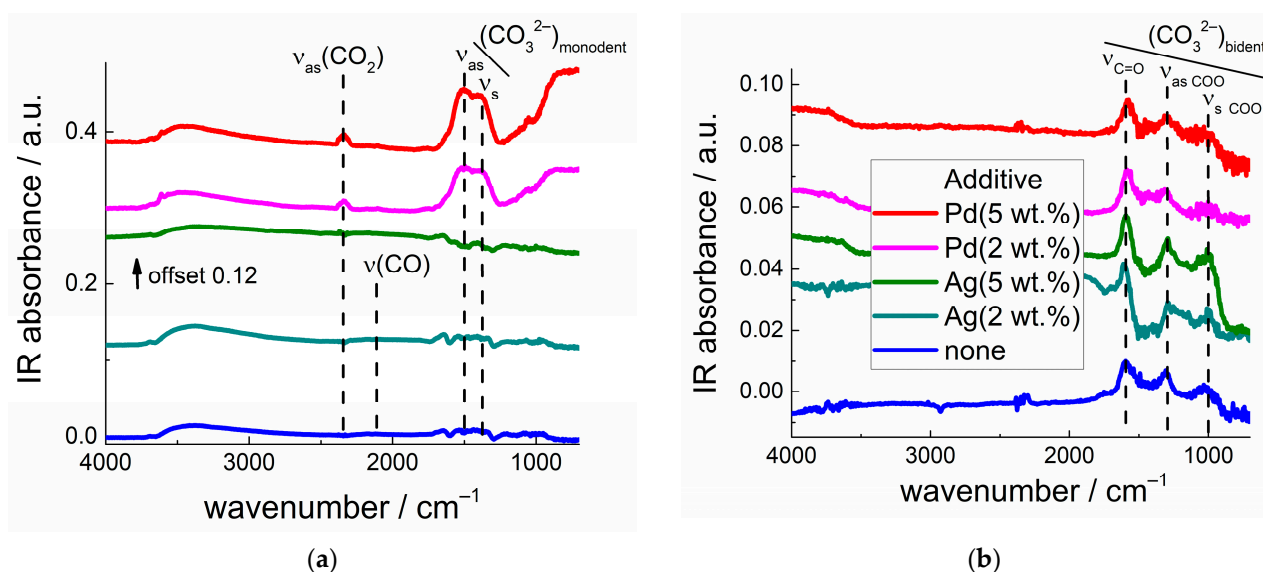
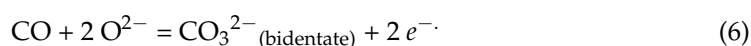


Figure 10. DRIFT spectra of pristine and Ag- or Pd-modified LaFeO₃ under exposure to 400 ppm CO for 1 h at room temperature (a) and at 200 °C (b).

The minor peak at 2100 cm⁻¹ observed in the DRIFT spectra of Pd-modified samples can be ascribed to the C-O stretching vibration of CO bound to Pd⁰ sites [28]. This agrees with our previous DRIFT observations that metal-oxide-supported Pd species specifically chemisorb CO at room temperature, which facilitates its oxidation by oxygen [39,40].

At a higher temperature (200 °C), the interaction with CO caused similar DRIFT spectral features for all samples (Figure 10b). The main one was the appearance of two positive peaks at 1580 cm⁻¹ and 1290 cm⁻¹ and a minor peak at 1000 cm⁻¹. The set of these peaks and their positions suggest their attribution to C=O stretching and asymmetric and symmetric COO stretching vibrations of bidentate carbonate, respectively [28]. In the wavenumber region below 800 cm⁻¹, a negative band can be observed. This implies the decreased intensity of metal–oxygen stretching vibrations in LaFeO₃, perhaps because oxygen anions at the perovskite surface are involved in the reaction with CO with the formation of bidentate carbonates:



The intensities of the positive CO₃²⁻ peaks and the negative M-O band in DRIFT spectra at higher temperatures were much larger for Ag-modified LaFeO₃ and increased with the percentage of Ag (Figure 10b). This evidences that the Ag modifier promotes the reaction of CO oxidation (Equation (6)) via the activation of surface oxygen anions. This agrees with the improved high-temperature sensitivity of LaFeO₃/Ag to CO and the growth in sensitivity with the percentage of Ag.

4. Discussion

In the present work, gas-sensitive nanocrystalline LaFeO₃ with a perovskite-like structure, a crystallite size of 19–28 nm and a BET surface area of 6–8 m²/g was synthesized using the sol–gel method. The materials were modified by Ag and Pd at concentrations of 2–5 wt.%, and the additives were deduced to be in the form of nanoparticles segregated at the surface of LaFeO₃. Noble metal additives were observed to be in mixed-valence partially oxidized states: Ag₂O/Ag with the predominance of metallic silver in LaFeO₃/Ag, and PdO/Pd with the prevalence of oxidized palladium in LaFeO₃/Pd. The difference might be due to the lower Ag–O bond energy and, hence, the lower stability of silver oxide in comparison to the Pd–O system [41]. Additionally, the larger fraction of reduced Ag could be due to the higher annealing temperature of AgNO₃-impregnated precursors (400 °C) than that of Pd(acac)₂-impregnated ones (300 °C). No incorporation of Ag⁺ or Pd²⁺

cations into the lattice of LaFeO₃ was deduced in the nanocomposites, since the positions of XRD peaks of LaFeO₃ did not shift in the presence of different Ag or Pd concentrations (Figure 1). Moreover, a significant discrepancy in the cationic radii rules out the formation of solid solutions in LaFeO₃/Ag or LaFeO₃/Pd materials: $r(\text{Ag}^+) = 1.15 \text{ \AA}$, $r(\text{Pd}^{2+}) = 0.86 \text{ \AA}$, $r(\text{Fe}^{3+}) = 0.65 \text{ \AA}$ (CN = 6), and $r(\text{La}^{3+}) = 1.32 \text{ \AA}$ (CN = 12) [42].

Comparing the sensor signals of pristine LaFeO₃ to different gases, a higher sensitivity to H₂S was observed (Figure 7). This can be attributed to the surface basicity of lanthanum ferrite. The low charges of the La³⁺ and Fe³⁺ cations and the relatively large radius of La³⁺ stipulate the basicity of surface oxygen anions, which is favorable for the interaction with acidic H₂S molecules. The sensitivity to other reducing gases (CO and NH₃) and the oxidizing gas NO₂ was comparable, showing the low, poor selectivity of LaFeO₃. The modification of LaFeO₃ with the additive Ag or Pd selectively improved the sensitivity to CO (Figure 8). Moreover, the temperature dependence of sensor signals of Pd-modified composites shifted to a lower temperature relative to LaFeO₃ and LaFeO₃/Ag (Figure 7). This can be utilized for the selective detection of CO by incorporating LaFeO₃/Ag and LaFeO₃/Pd sensors, operated at appropriate temperatures, into a multisensor device. The sensitivity to CO increased with the concentration of Ag and Pd in the composites, indicating that improved sensitivity and selectivity were induced by the noble metal additives. The values of sensor signals were not as high as can be reached by CO sensors based on binary oxides (SnO₂, TiO₂ or WO₃) and composites with noble metals [43]. However, among the sensors of CO based on perovskite mixed-metal oxides (Table 4), the present materials LaFeO₃/Ag and LaFeO₃/Pd showed the advantages of moderate operating temperatures, sensitivity to as low as 2 ppm CO, selectivity, and resistance to humidity.

From the results of in situ DRIFT spectroscopy, we deduced that the selective enhancement of the sensitivity to CO was controlled by the catalytic effects of Ag and Pd additives in the reaction of target gas oxidation at the surface of LaFeO₃. The difference in the optimal operating temperatures of Ag- and Pd-modified sensors was due to distinct sensing mechanisms inferred from DRIFT spectra of materials exposed to CO. It has often been stated in the literature that the sensing principle of semiconductor metal oxides relies on the ionosorption of oxygen in the form of O₂⁻, O⁻ or O²⁻ and the interaction of ionosorbed species with target gas molecules [2,3]. However, the existence of adsorbed oxygen species had hardly been proved experimentally at the surface of mixed-metal oxides such as perovskites. On the other hand, an alternate sensing mechanism considers the interaction of target gas molecules with lattice O²⁻ anions on the oxide surface, which results in the reversible formation and replenishment of oxygen vacancies. In certain cases, this model was found to be suitable for the description of gas sensing by certain metal oxides [44,45]. In the present work, we suggest that the mechanism of CO sensing is the interaction with lattice oxygen anions at the surface of LaFeO₃ (Equation (6)). Indirect evidence for this is the appearance of bidentate carbonate species at a temperature of 200 °C (DRIFT spectra in Figure 10b), corresponding to the conditions of the maximum sensor signals of pristine and Ag-modified LaFeO₃ (Figure 7). Furthermore, LaMO₃ perovskites, with M being a trivalent cation, are known as efficient catalysts in oxygen evolution reactions, and LaFeO₃ has a comparatively low energy of hole formation at oxygen anions [46]. This means that lattice O²⁻ anions in LaFeO₃ can be relatively easily transformed into reactive single charged and uncharged oxygen atoms, which is favorable for their reduction by reducing gas molecules such as CO.

In the presence of Ag₂O/Ag nanoparticles, the reaction of CO with oxygen anions at the surface of LaFeO₃ (Equation (6)) is enhanced but still requires a higher temperature (200 °C). This follows from the increased formation of bidentate CO₃²⁻ species in DRIFT spectra (Figure 10b) and from the improved sensor signals of LaFeO₃/Ag at the same operating temperature as for pristine LaFeO₃ (Figure 7). The activation of surface oxygen anions of LaFeO₃ by supported silver nanoparticles might proceed via the spillover effect, which has been assumed in the literature for noble-metal-modified sensors (the model of

chemical sensitization) [2] and was experimentally established by oxygen isotopic exchange on oxide-supported clusters of platinum-group metals [47,48].

The role of the Pd additive in the improved sensitivity to CO is also the catalysis of target gas conversion at the surface of LaFeO₃. However, in contrast to Ag-modified samples, Pd activates CO molecules for the oxidation reaction, rather than surface oxygen species. The specific chemisorption of CO on Pd sites, which takes place at as low as room temperature, loosens the C≡O triple bond due to π back-donation from Pd atoms and decreases the activation energy for CO conversion. This follows from the evolution of the characteristic peaks of CO₂ and monodentate carbonates in the DRIFT spectra at room temperature (Figure 10a) and accounts for the lowering of the optimal operating temperature of Pd-modified sensors in the detection of CO (Figure 7a). Since the conversion of CO over the Pd catalyst (Equations (2–5)) does not directly involve electrons from the semiconductor, high sensitivity to CO was not observed at room temperature. The concentration of the charge carrier could be influenced by the reduction of PdO to Pd and by the variation in the Schottky barrier height at the interface with LaFeO₃ (Figure 9), as was supported by the downward shift of baseline IR absorbance in DRIFT spectra (Figure 10a). However, no change in material resistance could be measured at low temperatures because of the relatively high activation energy of conduction of about 0.5–0.6 eV (Table 3). On the other hand, at a higher temperature (200 °C), the interaction of CO with LaFeO₃/Pd proceeded similarly to that with pristine LaFeO₃ (Equation (6)), since the observed peaks of bidentate carbonates had similar intensities in the DRIFT spectra (Figure 10b). Thus, the selectively improved sensitivity of LaFeO₃/Pd to CO at a moderate temperature (150 °C) was likely a compromise between the specific catalytic conversion of CO on Pd sites, which dominates at room temperature (Equations (2–5)), and the oxidation of CO by oxygen anions at the surface of LaFeO₃, which is predominant at higher temperatures (Equation (6)).

5. Conclusions

Nanocrystalline LaFeO₃ with a perovskite-like structure, a crystallite size of 19–28 nm and a specific surface area of 6–8 m²/g was synthesized using the sol–gel method. Nanocomposites of LaFeO₃ with different concentrations of Ag and Pd additives (2–5 wt.%) were obtained via impregnation. The additives were observed in the form of partially oxidized Ag₂O/Ag and PdO/Pd segregations at the surface of LaFeO₃. The electrical conduction and sensing behavior were studied. An increased activation energy of conduction was found in Ag- and Pd-modified samples due to the difference in work functions and the formation of Schottky barriers at the additive/perovskite interface. Selectively improved sensitivity to CO was observed for Ag- and Pd-modified LaFeO₃, provided with sensitivity to as low as 2 ppm CO, moderate operating temperatures (150–200 °C) and resistance to humidity. Different CO-sensing mechanisms of LaFeO₃/Ag and LaFeO₃/Pd were revealed using in situ diffuse-reflectance infrared spectroscopy. Ag activates oxygen anions at the surface of LaFeO₃ in the reaction of CO oxidation at a higher temperature (200 °C) and thus enhances the sensitivity. Pd catalyzes the oxidative conversion of CO via the specific chemisorption of target gas molecules, which results in improved sensitivity at a lower temperature (150 °C).

Supplementary Materials: The following supporting information can be downloaded at: <https://www.mdpi.com/article/10.3390/chemosensors11010060/s1>. Figure S1: X-ray fluorescence spectra of pristine LaFeO₃ and Ag-modified LaFeO₃ (a), and Pd-modified LaFeO₃ (b). Peaks of Zr correspond to anode of X-ray emitter tube. Figure S2: Enlarged FTIR spectra of the materials as in Figure 4 in the main text.

Author Contributions: Conceptualization, M.R.; methodology, V.C. and A.M.; investigation, V.C., A.M., V.P. and N.K.; resources, A.M., V.P. and M.R.; data curation, V.C., A.M. and V.P.; writing—original draft preparation, A.M.; writing—review and editing, M.R.; visualization, A.M.; supervision, M.R.; project administration, A.M.; funding acquisition, A.M. All authors have read and agreed to the published version of the manuscript.

Funding: This work was supported by a grant from Russian Science Foundation, No. 22-73-10038, <https://rscf.ru/project/22-73-10038/> (accessed on 3 January 2023).

Institutional Review Board Statement: Not applicable.

Informed Consent Statement: Not applicable.

Data Availability Statement: Not applicable.

Acknowledgments: The authors thank F. Spiridonov for technical support in the XRD experiments.

Conflicts of Interest: The authors declare no conflict of interest.

References

1. Gopel, W. Chemisorption and charge transfer at ionic semiconductor surfaces: Implications in designing gas sensors. *Prog. Surf. Sci.* **1985**, *20*, 9–103. [CrossRef]
2. Dey, A. Semiconductor metal oxide gas sensors: A review. *Mater. Sci. Eng. B* **2018**, *229*, 206–217. [CrossRef]
3. Shankar, P.; Bosco, J.; Rayappan, B. Gas sensing mechanism of metal oxides: The role of ambient atmosphere, type of semiconductor and gases—A review. *ScienceJet* **2015**, *4*, 126.
4. Enhessari, M.; Salehabadi, A. Perovskite-based materials for chemical sensors. In *Progresses in Chemical Sensor*; Wang, W., Ed.; IntechOpen: London, UK, 2016; pp. 59–91.
5. Fergus, J.W. Perovskite oxides for semiconductor-based gas sensors. *Sens. Actuators B Chem.* **2007**, *123*, 1169–1179. [CrossRef]
6. Pena, M.A.; Fierro, J.L.G. Chemical Structures and Performance of Perovskite Oxides. *Chem. Rev.* **2001**, *101*, 1981–2018. [CrossRef]
7. Tejuca, L.G.; Fierro, J.L.G. (Eds.) *Properties and Applications of Perovskite-Type Oxides*, 1st ed.; CRC Press: Boca Raton, FL, USA, 1993; pp. 241–267.
8. Balamurugan, C.; Song, S.-J.; Kim, H.-S. Enhancing Gas Response Characteristics of Mixed Metal Oxide Gas Sensors. *J. Korean Ceram. Soc.* **2018**, *55*, 1–20. [CrossRef]
9. Yu, J.; Xiang, S.; Ge, M.; Zhang, Z.; Huang, J.; Tang, Y.; Sun, L.; Lin, C.; Lai, Y. Rational Construction of LaFeO₃ Perovskite Nanoparticle-Modified TiO₂ Nanotube Arrays for Visible-Light Driven Photocatalytic Activity. *Coatings* **2018**, *8*, 374–384. [CrossRef]
10. Wheeler, G.; Choi, K.-S. Photoelectrochemical Properties and Stability of Nanoporous p-Type LaFeO₃ Photoelectrodes Prepared by Electrodeposition. *ACS Energy Lett.* **2017**, *2*, 2378–2382. [CrossRef]
11. Li, X.; Li, Z.; Lu, C.; Li, D.; Li, Z.; Gao, J.; Wei, J.; Li, K. Enhanced performance of LaFeO₃ oxygen carriers by NiO for chemical looping partial oxidation of methane. *Fuel Process. Technol.* **2022**, *236*, 107396. [CrossRef]
12. Gu, J.; Zhang, B.; Li, Y.; Xu, X.; Sun, G.; Cao, J.; Wang, Y. Synthesis of spindle-like Co-doped LaFeO₃ porous microstructure for high performance n-butanol sensor. *Sens. Actuators B Chem.* **2021**, *343*, 130125. [CrossRef]
13. Zhang, X.; Zhang, W.-L.; Cai, Z.-X.; Li, Y.-K.; Yamauchi, Y.; Guo, X. LaFeO₃ porous hollow micro-spindles for NO₂ sensing. *Ceram. Int.* **2019**, *45*, 5240–5248. [CrossRef]
14. Bai, S.; Shi, B.; Ma, L.; Yang, P.; Liu, Z.; Li, D.; Chen, A. Synthesis of LaFeO₃ catalytic materials and their sensing properties. *Sci. China Ser. B Chem.* **2009**, *52*, 2106–2113. [CrossRef]
15. Fan, H.; Zhang, T.; Xu, X.; Lu, N. Fabrication of N-type Fe₂O₃ and P-type LaFeO₃ nanobelts by electrospinning and determination of gas-sensing properties. *Sens. Actuators B Chem.* **2011**, *153*, 83–88. [CrossRef]
16. Queralto, A.; Graf, D.; Frohnhoven, R.; Fischer, T.; Vanrompay, H.; Bals, S.; Bartasyte, A.; Mathur, S. LaFeO₃ nanofibers for high detection of sulfur-containing gas. *ACS Sustain. Chem. Eng.* **2019**, *7*, 6023–6032. [CrossRef]
17. Zhang, Y.M.; Lin, Y.T.; Chen, J.L.; Zhang, J.; Zhu, Z.Q.; Liu, Q.J. A high sensitivity gas sensor for formaldehyde based on silver doped lanthanum ferrite. *Sens. Actuators B Chem.* **2014**, *190*, 171–176. [CrossRef]
18. Wang, C.; Rong, Q.; Zhang, Y.; Hu, J.; Zi, B.; Zhu, Z.; Zhang, J.; Liu, Q. Molecular imprinting Ag-LaFeO₃ spheres for highly sensitive acetone gas detection. *Mater. Res. Bull.* **2019**, *109*, 265–272. [CrossRef]
19. Alharbi, A.A.; Sackmann, A.; Weimar, U.; Barsan, N. Acetylene- and Ethylene-Sensing Mechanism for LaFeO₃-Based Gas Sensors: Operando Insights. *J. Phys. Chem. C* **2020**, *124*, 7317–7326. [CrossRef]
20. Thirumalairajan, S.; Girija, K.; Mastelaro, V.R.; Ponpandian, N. Surface Morphology-Dependent Room-Temperature LaFeO₃ Nanostructure Thin Films as Selective NO₂ Gas Sensor Prepared by Radio Frequency Magnetron Sputtering. *ACS Appl. Mater. Interfaces* **2014**, *6*, 13917–13927. [CrossRef]
21. Ding, J.-C.; Li, H.-Y.; Cai, Z.-X.; Wang, X.-X.; Guo, X. Near room temperature CO sensing by mesoporous LaCoO₃ nanowires functionalized with Pd nanodots. *Sens. Actuators B Chem.* **2016**, *222*, 517–524. [CrossRef]
22. Navale, S.; Shahbaz, M.; Mirzaei, A.; Kim, S.S.; Kim, H.W. Effect of Ag Addition on the Gas-Sensing Properties of Nanostructured Resistive-Based Gas Sensors: An Overview. *Sensors* **2021**, *21*, 6454. [CrossRef]
23. Thirumalairajan, S.; Girija, K.; Hebalkar, N.Y.; Mangalaraj, D.; Viswanathan, C.; Ponpandian, N. Shape evolution of perovskite LaFeO₃ nanostructures: A systematic investigation of growth mechanism, properties and morphology dependent photocatalytic activities. *RSC Adv.* **2013**, *3*, 7549–7561. [CrossRef]

24. Li, X.; Zhang, H.; Liu, X.; Li, S.; Zhao, M. XPS study on O(1s) and Fe(2p) for nanocrystalline composite oxide LaFeO₃ with the perovskite structure. *Mater. Chem. Phys.* **1994**, *38*, 355–362. [CrossRef]
25. Ferrara, A.M.; Carapeto, A.P.; Botelho do Rego, A.M. X-ray photoelectron spectroscopy: Silver salts revisited. *Vacuum* **2012**, *86*, 1988–1991. [CrossRef]
26. Cao, K.; Cao, E.; Zhang, Y.; Hao, W.; Sun, L.; Peng, H. The influence of nonstoichiometry on electrical transport and ethanol sensing characteristics for nanocrystalline LaFe_xO_{3-δ} sensors. *Sens. Actuators B Chem.* **2016**, *230*, 592–599. [CrossRef]
27. Sharma, N.; Kushwaha, H.S.; Sharma, S.K.; Sachdev, K. Fabrication of LaFeO₃ and rGO-LaFeO₃ microspheres based gas sensors for detection of NO₂ and CO. *RSC Adv.* **2020**, *10*, 1297–1308. [CrossRef]
28. Hadjiivanov, K.I.; Vayssilov, G.N. Characterization of Oxide Surfaces and Zeolites by Carbon Monoxide as an IR Probe Molecule. *Adv. Catal.* **2002**, *47*, 307–511.
29. Kofenstein, R.; Jager, L.; Ebbinghaus, S.G. Magnetic and optical investigations on LaFeO₃ powders with different particle sizes and corresponding ceramics. *Solid State Ion.* **2013**, *249–250*, 1–5. [CrossRef]
30. Seo, J.W.; Fullerton, E.E.; Nolting, F.; Scholl, A.; Fompeyrine, J.; Locquet, J.-P. Antiferromagnetic LaFeO₃ thin films and their effect on exchange bias. *J. Phys. Condens. Matter* **2008**, *20*, 264014. [CrossRef]
31. Smolin, S.Y.; Choquette, A.K.; Wilks, R.G.; Gauquelin, N.; Félix, R.; Gerlach, D.; Ueda, S.; Krick, A.L.; Verbeeck, J.; Bär, M.; et al. Energy Level Alignment and Cation Charge States at the LaFeO₃/LaMnO₃ (001) Heterointerface. *Adv. Mater. Interfaces* **2017**, *4*, 1700183. [CrossRef]
32. Hong, J.-P.; Park, A.-Y.; Lee, S.; Kang, J.; Shin, N.; Yoon, D.Y. Tuning of Ag work functions by self assembled monolayers of aromatic thiols for an efficient hole injection for solution processed triisopropylsilylethynyl pentacene organic thin film transistors. *Appl. Phys. Lett.* **2008**, *92*, 143311. [CrossRef]
33. Magari, Y.; Makino, H.; Hashimoto, S.; Furuta, M. Origin of work function engineering of silver oxide for an In–Ga–Zn–O Schottky diode. *Appl. Surf. Sci.* **2020**, *512*, 144519. [CrossRef]
34. Jaeckel, R.; Wagner, B. Photo-electric measurement of the work function of metals and its alteration after gas adsorption. *Vacuum* **1963**, *13*, 509–511. [CrossRef]
35. OSHA. Occupational Chemical Database. Available online: <https://www.osha.gov/chemicaldata/462> (accessed on 9 December 2022).
36. Toan, N.; Saukko, S.; Lantto, V. Gas sensing with semiconducting perovskite oxide LaFeO₃. *Phys. B Condens. Mater.* **2003**, *327*, 279–282. [CrossRef]
37. Murade, P.A.; Sangawar, V.S.; Chaudhari, G.N.; Kapse, V.D.; Bajpeyee, A.U. Acetone gas-sensing performance of Sr-doped nanostructured LaFeO₃ semiconductor prepared by citrate sol-gel route. *Curr. Appl. Phys.* **2011**, *11*, 451–456. [CrossRef]
38. Liu, H.; Sun, H.; Xie, R.; Zhang, X.; Zheng, K.; Peng, T.; Wuc, X.; Zhang, Y. Substrate-dependent structural and CO sensing properties of LaCoO₃ epitaxial films. *Appl. Surf. Sci.* **2018**, *442*, 742–749. [CrossRef]
39. Marikutsa, A.; Yang, L.; Rummyantseva, M.; Batuk, M.; Hadermann, J.; Gaskov, A. Sensitivity of nanocrystalline tungsten oxide to CO and ammonia gas determined by surface catalysts. *Sens. Actuators B Chem.* **2018**, *277*, 336–346. [CrossRef]
40. Marikutsa, A.; Rummyantseva, M.; Gaskov, A. Specific Interaction of PdO_x- and RuO_y-Modified Tin Dioxide with CO and NH₃ Gases: Kelvin Probe and DRIFT Studies. *J. Phys. Chem. C* **2015**, *119*, 24342–24350. [CrossRef]
41. Moltved, K.A.; Kepp, K.P. The Chemical Bond between Transition Metals and Oxygen: Electronegativity, d-Orbital Effects, and Oxophilicity as Descriptors of Metal–Oxygen Interactions. *J. Phys. Chem. C* **2019**, *123*, 18432–18444. [CrossRef]
42. Shannon, R.D. Revised effective ionic radii and systematic studies of interatomic distances in halides and chalcogenides. *Acta Cryst.* **1976**, *A32*, 751–767. [CrossRef]
43. Mahajan, S.; Jagtap, S. Metal-oxide semiconductors for carbon monoxide (CO) gas sensing: A review. *Appl. Mater. Today* **2020**, *18*, 100483. [CrossRef]
44. Degler, D.; Wicker, S.; Weimar, U.; Barsan, N. Identifying the Active Oxygen Species in SnO₂ Based Gas Sensing Materials: An Operando IR Spectroscopy Study. *J. Phys. Chem. C* **2015**, *119*, 11792–11799. [CrossRef]
45. Staerz, A.; Weimar, U.; Barsan, N. Current state of knowledge on the metal oxide based gas sensing mechanism. *Sens. Actuators B Chem.* **2022**, *358*, 131531. [CrossRef]
46. Yang, C.; Grimaud, A. Factors Controlling the Redox Activity of Oxygen in Perovskites: From Theory to Application for Catalytic Reactions. *Catalysts* **2017**, *7*, 149. [CrossRef]
47. Sadovskaya, E.M.; Ivanova, Y.A.; Pinaeva, L.G.; Grasso, G.; Kuznetsova, T.G.; van Veen, A.; Sadykov, V.A.; Mirodatos, C. Kinetics of Oxygen Exchange over CeO₂-ZrO₂ Fluorite-Based Catalysts. *J. Phys. Chem. A* **2007**, *111*, 4498–4505. [CrossRef]
48. Martin, D.; Duprez, D. Mobility of Surface Species on Oxides. 1. Isotopic Exchange of ¹⁸O₂ with ¹⁶O of SiO₂, Al₂O₃, ZrO₂, MgO, CeO₂, and CeO₂-Al₂O₃. Activation by Noble Metals. Correlation with Oxide Basicity. *J. Phys. Chem.* **1996**, *100*, 9429–9438. [CrossRef]

Disclaimer/Publisher’s Note: The statements, opinions and data contained in all publications are solely those of the individual author(s) and contributor(s) and not of MDPI and/or the editor(s). MDPI and/or the editor(s) disclaim responsibility for any injury to people or property resulting from any ideas, methods, instructions or products referred to in the content.